Chemical Geology 381 (2014) 55–66

Contents lists available at ScienceDirect

Chemical Geology

journal homepage: www.elsevier.com/locate/chemgeo

New insights into cerium anomalies and mechanisms of trace metal enrichment in authigenic carbonate from hydrocarbon seeps

Yu Hu [a,e], Dong Feng [b,*], Jörn Peckmann [c], Harry H. Roberts [d], Duofu Chen [a,b,**]

[a] CAS Key Laboratory of Marginal Sea Geology, Guangzhou Institute of Geochemistry, Chinese Academy of Sciences, Guangzhou 510640, China
[b] CAS Key Laboratory of Marginal Sea Geology, South China Sea Institute of Oceanology, Chinese Academy of Sciences, Guangzhou 510301, China
[c] Department of Geodynamics and Sedimentology, Center for Earth Sciences, University of Vienna, 1090 Vienna, Austria
[d] Coastal Studies Institute, Department of Oceanography and Coastal Sciences, Louisiana State University, Baton Rouge, LA 70803, USA
[e] University of Chinese Academy of Sciences, Beijing 100049, China

ARTICLE INFO

Article history:
Received 29 December 2013
Received in revised form 3 April 2014
Accepted 3 May 2014
Available online 21 May 2014

Editor: Michael E. Böttcher

Keywords:
Hydrocarbon seeps
Authigenic carbonates
Rare earth elements
Trace metals
Redox conditions
Trace metal enrichments

ABSTRACT

Authigenic carbonates that form at marine hydrocarbon seeps provide a unique geological archive of past local environmental conditions and pore fluid geochemistry. Recent work on such carbonates revealed variable cerium (Ce) anomalies and anomalous enrichments of certain trace metals. However, the mechanisms accounting for such anomalies remain poorly constrained. Here, we characterize the rare earth element (REE) patterns of carbonate phases and the trace metal patterns of bulk carbonate rocks sampled at three hydrocarbon seeps located at Congo Fan pockmarks (CF) and the Gulf of Mexico sites AC645 and GB425. The analyzed CF, GB425, and AC645 carbonates yielded different REE patterns, displaying positive, no, as well as negative Ce anomalies. The covariation of molybdenum (Mo) with uranium (U), including authigenic Mo (Mo_{auth}) and U (U_{auth}) enrichments as well as $(Mo/U)_{auth}$ ratios proved useful to obtain new insight into the applicability of Ce anomalies to constrain past redox conditions. Trace element patterns suggest that (1) CF carbonates formed in a restricted sulfidic environment, while (2) the AC645 site experienced intermittent oxygenation causing negative Ce anomalies, and (3) environmental conditions were variable at the GB425 mud volcano site. Interestingly, GB425 carbonates show significant Mo, arsenic (As), and antimony (Sb) enrichments with the enrichment factor of As (As_{EF}) correlating well with the authigenic Fe fraction. These results suggest that iron oxyhydroxides played an important role in the adsorption of Mo, As, and Sb in the water column and their transfer to the sediment. The combination of trace metal and REE geochemistry of authigenic carbonates used here is a promising tool to better assess past variability of redox conditions and biogeochemical processes at marine hydrocarbon seeps.

1. Introduction

Seepage of hydrocarbon-rich fluids mainly consisting of methane out of the sedimentary column is a widespread phenomenon along continental margins worldwide (Campbell, 2006; Judd and Hovland, 2007 and references therein). Seafloor expressions of focused fluid seepage include a large range of geological structures such as gas chimneys, pockmarks, mud volcanoes, and brine pools (Judd and Hovland, 2007 and references therein). Modern marine hydrocarbon seeps are characterized by highly variable seepage intensity (Tryon et al., 1999; Klaucke et al., 2010), resulting in significant changes of chemical and physical parameters and early diagenetic conditions within sediments (Tryon et al., 1999; Tryon and Brown, 2004; Solomon et al., 2008). At seeps, methane is mostly consumed within sediments by sulfate-dependent anaerobic oxidation of methane (AOM) mediated by a microbial consortium (Hinrichs et al., 1999; Boetius et al., 2000). This process releases dissolved bicarbonate and hydrogen sulfide, thereby increasing pore water alkalinity, thus favoring precipitation of authigenic carbonate close to the seafloor (Berner, 1980). The resultant authigenic carbonates provide excellent geological and geochemical archives to evaluate the conditions of mineral formation, the evolution of pore fluids, and the biogeochemical processes at seeps (Roberts and Carney, 1997; Bohrmann et al., 1998; Greinert et al., 2001; Peckmann et al., 2001; Peckmann and Thiel, 2004; Roberts et al., 2010a).

Rare earth elements (REE) have been frequently used to trace changes in the composition of seep fluids and to assess redox conditions during the formation of seep carbonates (Chen et al., 2005; Feng et al., 2009a,b, 2010a; Ge et al., 2010; Himmler et al., 2010; Bayon et al., 2011; Birgel et al., 2011; Rongemaille et al., 2011; Kim et al., 2012; Bayon et al., 2013; Feng et al., 2013; Himmler et al., 2013). Some of

* Corresponding author. Tel.: +86 20 85290286; fax: +86 20 85290130.
** Correspondence to: D. Chen, CAS Key Laboratory of Marginal Sea Geology, Guangzhou Institute of Geochemistry, Chinese Academy of Sciences, Guangzhou 510640, China. Tel.: +86 20 85290286; fax: +86 20 85290130.
E-mail addresses: feng@scsio.ac.cn (D. Feng), cdf@gig.ac.cn (D. Chen).

http://dx.doi.org/10.1016/j.chemgeo.2014.05.014
0009-2541/

the studies on the REE geochemistry of seep carbonates revealed varying redox conditions during mineral formation (Feng et al., 2009a, b; Birgel et al., 2011). In particular, Birgel et al. (2011) suggested that temporarily oxic conditions prevailed based on real negative Ce anomalies and the presence of molecular fossils of aerobic methanotrophic bacteria. However, highly alkaline, organic-rich pore fluids may also cause the generation of negative Ce anomalies (Pourret et al., 2008; Kim et al., 2012). To better constrain paleoenvironments and paleoredox conditions, trace metals, including redox-sensitive elements such as uranium (U) and molybdenum (Mo) that are strongly enriched under anoxic conditions, are commonly used (Algeo and Tribovillard, 2009; Tribovillard et al., 2012a,b). Uranium and Mo exhibit conservative behavior under oxic conditions and have long residence times in seawater (~450 kyr for U, ~780 kyr for Mo), while both elements are enriched in authigenic mineral phases under reducing conditions (Algeo and Tribovillard, 2009). In oxic seawater, U is present mainly as U(VI), forming $UO_2(CO_3)_3^{4-}$, and Mo is adsorbed onto manganese oxyhydroxides (Tribovillard et al., 2006). Under suboxic conditions close to the Fe(III)–Fe(II) transition, soluble U(VI) is reduced to insoluble U(IV), the uptake of which may be accelerated by the presence of organic substrates (Zheng et al., 2002; Tribovillard et al., 2006; Algeo and Tribovillard, 2009). Under such conditions, the rate of accumulation of authigenic U (U_{auth}) increases relative to that of authigenic Mo (Mo_{auth}), resulting in $(Mo/U)_{auth}$ ratios of sediment that are below those of seawater (Algeo and Tribovillard, 2009). As the sedimentary environment becomes increasingly reducing with free hydrogen sulfide being generated, molybdate (MoO_4^{2-}) is converted to thiomolybdates ($MoS_{4-x}O_x^{2-}$) that are scavenged from solution via organic material or via Mo capture by iron sulfide phases (Helz et al., 1996; Zheng et al., 2000; Tribovillard et al., 2006; Helz et al., 2011). Under such conditions, Mo_{auth} enrichment tends to exceed that of U_{auth} and $(Mo/U)_{auth}$ ratios of sediment equal or exceed ratios of seawater (Algeo and Tribovillard, 2009). Therefore, authigenic U–Mo enrichment and their covariation patterns in marine sediments are a robust proxy for tracing variation of redox condition. The patterns of authigenic U–Mo covariation as a redox indicator have already been employed in the study of seep carbonates and sediments (Palomares et al., 2012; Sato et al., 2012). However, such trace-metal studies focusing on the reconstruction of the conditions during mineral formation at seeps have rarely been combined with REE geochemistry, yet, the combination of trace-metal and REE studies has great potential to shed new light on the causes of Ce anomalies and past environmental conditions.

Trace metals have the potential to serve as tracer for the source of seep fluids. For instance, Nath et al. (2008) reported elevated levels of arsenic (As) in mud volcano fluids. Similar As enrichment, as well as Mo and antimony (Sb) anomalies have been observed in seep sediments from an active mud volcano (Cangemi et al., 2010). The enrichments of trace metals have been attributed to the ascending fluids from deep sedimentary strata (Nath et al., 2008; Cangemi et al., 2010). Similarly, Mo, As, and Sb enrichments have also been found in ancient seep carbonates, however, the overlying seawater was considered to have been responsible for the trace-metal enrichments through a so-called iron–manganese-oxyhydroxide shuttle (Tribovillard et al., 2013).

Similar trace-metal enrichments are also present in some of the seep carbonates studied here, which were collected from an active mud volcano situated at Garden Banks block 425 (GB425, Gulf of Mexico), representing a good opportunity to explore possible enrichment mechanisms. Seep carbonates from two other sites (Congo Fan off western Africa and Alaminos Canyon block 645, Gulf of Mexico) were used to obtain new insight into the causes of Ce anomalies. Here, REE signatures of individual, authigenic carbonate phases as well as trace element compositions of bulk seep carbonate rocks are presented to explore the mechanisms that cause anomalies of certain elements, allowing to further constrain the formation conditions of seep carbonates and the involved geochemical processes.

2. Geological background

2.1. Congo Fan

The northern Congo Fan is located offshore western Africa on the Congo–Angolan margin, which is a passive continental margin resulting from the Early Cretaceous opening of the South Atlantic Ocean (130 Ma; Marton et al., 2000). After 1000 m thick evaporites accumulated in the Early Cretaceous, black shales and bituminous sandstones deposited during the middle Cretaceous (Droz et al., 1996). The terrigenous sediment input to the Atlantic Ocean increased strongly during the Cenozoic, resulting in the initiation of the huge Congo turbiditic sedimentation system and the formation of the Congo Fan (Droz et al., 1996). Numerous investigations on the Congo Fan revealed prominent features of focused upward fluid migration such as pockmarks (Charlou et al., 2004; Gay et al., 2006, 2007; Sahling et al., 2008; Haas et al., 2010; Nöthen and Kasten, 2011). Among other sites, the distribution of chemosynthesis-based communities, authigenic carbonates, and gas hydrates has been described from the Kouilou pockmarks located north of the Congo Fan (Sahling et al., 2008; Haas et al., 2010; Nöthen and Kasten, 2011).

2.2. Northern Gulf of Mexico

The northern Gulf of Mexico (GOM) is characterized by a column of over 10 km of Mesozoic–Cenozoic sediment that resulted in the generation and accumulation of large oil and gas reservoirs (Sassen and MacDonald, 1994). Extensive salt diapirism and related sediment deformation created faults, which provide efficient conduits for hydrocarbon fluid and gas migration from the deep subsurface petroleum systems into shallow sediments or to the seafloor (Sassen and MacDonald, 1994). Massive leakage of oil and gas from hydrocarbon traps manifests itself at the seafloor and in the water column as gas plumes, gas hydrate, oil-stained sediments, authigenic carbonates, and hydrocarbon-driven chemosynthesis-based communities (Roberts and Aharon, 1994; Aharon et al., 1997; Roberts and Carney, 1997; Sassen et al., 1999; Feng et al., 2009b). The Alaminos Canyon (AC) area is situated along a series of northeast–southwest trending salt-cored box folds of the Perdido fold belt located in the northwestern GOM (Trudgill et al., 1999). The AC645 site is a small mound surrounded by hemipelagic mud with no evidence of currently active hydrocarbon seepage; however, the mound is composed of imbricated slabs and blocks of seep carbonates (Roberts et al., 2010b). Garden Bank 425 (GB425) is a brine-charged site located in the northern GOM. Overpressured fluids migrating along faults above salt structures resulted in the formation of the GB425 mud volcanoes (Milkov and Sassen, 2000; Castellini et al., 2006), which is characterized by intense venting of hydrocarbon-rich brines (Joye et al., 2005) and the development of barite-rich carbonate nodules (Castellini et al., 2006).

3. Samples and methods

Considering different geological settings (e.g. pockmarks and mud volcanoes) and different, previously reported Ce anomalies (cf. Feng et al., 2010a; Birgel et al., 2011), authigenic carbonates from three seep sites on the Congo Fan and the GOM were chosen in this study (Fig. 1). Congo Fan (CF) carbonates were collected by TV-guided grabs from the Hydrate Hole and Diapir Field sites during RV METEOR Cruise M56. The AC645 carbonate samples were collected during dives with deep submergence vehicle (DSV) Alvin in 1990 (Dive 2209) and 2006 (Dives 4194 and 4197). The GB425 carbonates were collected from the southern venting sites of the mud volcano during an expedition with DSV Alvin (Dive 4645) in 2010. Location, geographical coordinates, water depth, $\delta^{13}C_{carbonate}$ values, and mineralogy of carbonate samples are listed in Table 1. Authigenic carbonates from the Congo Fan are mainly composed of aragonite and high-Mg calcite associated with

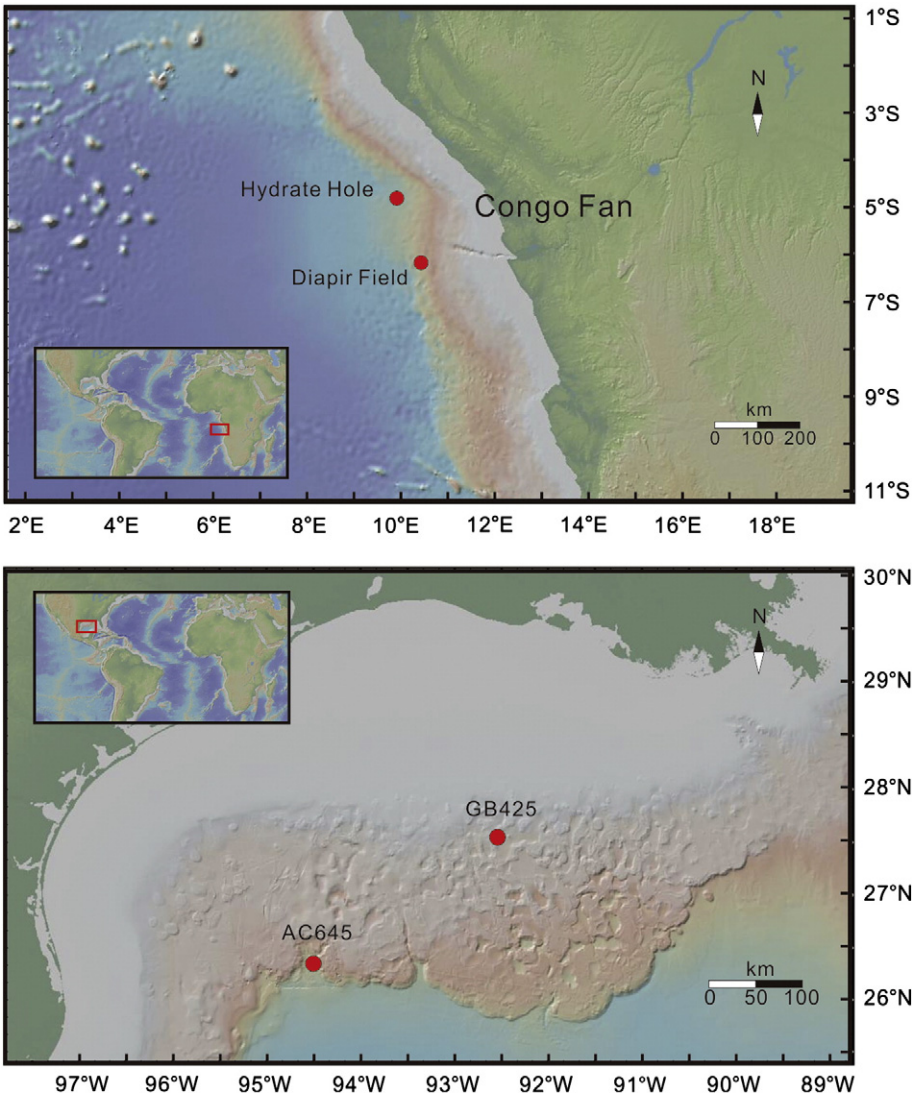

Fig. 1. Map showing the study locations of Congo Fan, Alaminos Canyon block 645 (AC645) and Garden Banks block 425 (GB425) in the Gulf of Mexico. Maps were created using GeoMapApp software.

abundant pyrite framboids enclosed in carbonate matrix (Feng et al., 2010a). The AC645 carbonate samples are characterized by almost pure aragonite, dense bivalve shells, and a porous texture (Feng et al., 2008; Birgel et al., 2011). The GB425 carbonates mainly consist of low-Mg calcite.

The carbonate samples were washed with deionized water immediately after collection and were subsequently air dried. The powdered samples for REE, major and trace element analysis were taken from slabs with a hand-held dental drill (ROTEX™ 782E). Carbonate samples were dissolved in (1) 5% acetic acid solutions for REE analysis of

Table 1
Location, geographical coordinates, water depth, $\delta^{13}C_{carbonate}$ values (‰ VPDB), and mineralogy of authigenic carbonate samples analyzed in this study.

Location	Latitude	Longitude	Water depth (m)	Morphology of carbonate precipitates	$\delta^{13}C$ (‰ VPDB)	Mineral composition			Reference
						Major	Minor	Trace	
Congo Fan									
Hydrate Hole	04°48.933′ S	09°54.833′ E	3100	Nodules, crusts, slabs, tubes, and filled molds	−62.5 to −46.3	Ara/HMC		Kao, Qz, Bar	Feng et al. (2010a); Haas et al. (2010)
Diapir Field	06°11.067′ S	10°25.833′ E	2400	Nodules, crusts and slabs	−40.7 to −30.7	Ara	HMC	Kao, Qz	Feng et al. (2010a); Haas et al. (2010)
Gulf of Mexico									
AC645	26°21.102′ N 26°21.240′ N	94°30.300′ W 94°29.802′ W	2230	Blocks, slabs and crusts	−33.9 to −22.2	Ara		HMC	Feng et al. (2008); Roberts et al. (2010a)
GB425	27°33.189′ N	92°32.450′ W	600	Nodules	−32.1 to −22.4	LMC	Sme	Qz, Dol	This study

Ara = aragonite, HMC = high-Mg calcite, LMC = low-Mg calcite, Bar = barite, Qz = quartz, Kao = kaolinite, Sme = smectite, Dol = dolomite.

authigenic minerals and (2) HF–HNO_3 solutions for major and trace element analysis of the whole rocks. For REE analyses, about 50 mg of powdered sample was weighed in Teflon beakers and leached by an ultra-pure solution of 5% acetic acid for 2 h to separate carbonate mineral and residue phases. The obtained solutions were centrifuged immediately after carbonate dissolution, and then evaporated on a hotplate until dry. Finally, the samples were dissolved in 3% HNO_3 spiked with an internal Rh standard (10 ppb) for REE analysis using a Perkin-Elmer Sciex ELAN 6000 ICP-MS. In this paper, $Ce/Ce^* = 3Ce_N / (2La_N + Nd_N)$, $Ce_{anom} = Log\ (Ce/Ce^*)$, $Eu/Eu^* = 2Eu_N / (Sm_N + Gd_N)$, and $Pr/Pr^* = 2Pr_N / (Ce_N + Nd_N)$, where N refers to normalization of concentration against the Post Archean Australian Shale (PAAS; McLennan, 1989).

Samples for major and trace element analysis of whole rocks were placed in Teflon beakers, dissolved by 1 ml of HF and 1 ml of HNO_3. The sealed beakers were then placed in an electric oven and heated to 185 °C for about 36 h. The beakers were heated on a hot plate to evaporate to dryness after cooling, and then 2 ml of HNO_3 and 3 ml of water were added. The beakers were sealed again and placed in an electric oven at 135 °C for about 5 h to dissolve the residue. Major elements were determined using a Varian Vista Pro ICP-AES. Trace elements were determined using a Perkin-Elmer Sciex ELAN 6000 ICP-MS. All the samples were analyzed at the Institute of Geochemistry, CAS. Certified reference materials (GSR-1, OU-6, 1633-a, GXR-2, GXR-5) were used for quality control. Precision and accuracy were both better than 5% for major elements, REE, and U, 10% for Mo, and 15% for As and Sb. To compare the respective authigenic enrichment of trace metals during seep carbonate formation, enrichment factors (EF) were used and defined as following: $X_{EF} = [(X / Al)_{sample} / (X / Al)_{reference}]$, where X and Al represent the weight concentrations of elements X and Al, respectively. Samples were normalized using the Post Archean Australian Shale (PAAS) compositions (Taylor and McLennan, 1985) or the Earth's upper crust (crust) compositions (McLennan, 2001). Although Al normalization has some potential pitfalls, enrichment factors are useful for the assessment of the authigenic fraction of trace metals (Tribovillard et al., 2006). In practice, $X_{EF} > 3$ represents a detectable authigenic enrichment and $X_{EF} > 10$ represents a moderate to strong enrichment (Algeo and Tribovillard, 2009).

4. Results

4.1. Rare earth elements

The total REE (ΣREE) contents of the studied seep carbonates range from 1.9 ppm to 27.0 ppm. Among the samples, CF carbonates exhibit the highest REE concentrations (ΣREE from 7.2 ppm to 27.0 ppm), followed by GB425 carbonates (11.6 ppm to 15.9 ppm), and AC645 samples (1.9 ppm to 4.3 ppm; Table 2 and Fig. 2). Carbonate samples of CF, GB425, and AC645 display real positive Ce anomalies ($Ce/Ce^* > 1.2$), no Ce anomalies, and real negative Ce anomalies ($Ce/Ce^* < 0.8$), respectively (Fig. 3). The Eu anomaly observed in CF and GB425 samples is due to the interference of BaO on Eu during ICP-MS analysis (Qi et al., 2005). Moderate middle REE (MREE) enrichments were observed in GB425 carbonates.

4.2. Major and trace elements

4.2.1. Major elements

Major element data are listed in Appendix 1. The highest average contents of Al_2O_3 are encountered in GB425 samples (mean 2.47 wt.%), followed by CF samples (mean 1.47%) and AC645 samples (mean 1.07%). Most of the AC645 samples have low Al_2O_3 contents that are below 0.33%. The Fe_2O_3 contents of GB425 samples vary from 1.88% to 7.44%, significantly higher than contents of CF and AC645 samples. MnO_2 contents of GB425 samples (mean 0.19%) are one order of magnitude higher than those of CF (mean 0.01%) and AC645 samples (mean 0.01%).

4.2.2. Trace elements

The average Mo concentrations decrease from CF (2.6–14.9 ppm; mean 6.2 ppm), over GB425 (1.0–7.6 ppm; mean 2.6 ppm) to AC645 samples (0.8–2.9 ppm; mean 1.6 ppm). Uranium concentrations are even more variable, ranging from 0.9 to 13.2 ppm (mean 4.2 ppm) in GB425, 2.6 to 6.5 ppm (mean 4.6 ppm) in AC645, and 1.8 to 12.0 ppm (mean 5.1 ppm) in CF samples (see Appendix 2). Arsenic and Sb are extremely enriched in GB425 samples relative to CF and AC645 samples. The average As concentrations in GB425 samples are as high as 27.9 ppm with maxima up to 140.0 ppm. High Sb concentrations are also

Table 2
Rare earth element, Mo and U contents (ppm) of authigenic carbonate phases in the carbonate rocks.

Sample ID	GeoB8212-2a-			GeoB8215-2c	GeoB8212-2d	AC645-			GB425-			
	1	2	3			4197-1	2209-ce[(a)]	4197-1-mi[(b)]	a	b	c	d
La	3.92	1.17	2.41	4.80	1.68	0.59	0.59	0.99	2.31	3.12	3.08	2.54
Ce	13.21	3.89	7.92	12.46	5.75	0.60	0.54	1.56	4.66	6.36	6.43	5.13
Pr	0.98	0.28	0.56	1.03	0.39	0.09	0.12	0.21	0.48	0.65	0.63	0.52
Nd	3.92	1.07	2.18	4.27	1.51	0.37	0.50	0.80	2.02	2.63	2.67	2.16
Sm	0.80	0.22	0.44	0.90	0.32	0.06	0.10	0.17	0.45	0.60	0.62	0.47
Eu	0.25	0.09	0.18	0.25	0.24	0.02	0.02	0.04	0.47	0.50	0.58	0.53
Gd	0.71	0.18	0.39	0.92	0.28	0.06	0.10	0.17	0.43	0.58	0.61	0.48
Tb	0.11	0.03	0.06	0.14	0.04	0.01	0.02	0.02	0.07	0.09	0.09	0.07
Dy	0.54	0.13	0.28	0.85	0.20	0.05	0.10	0.14	0.31	0.45	0.47	0.35
Ho	0.10	0.02	0.05	0.18	0.04	0.01	0.02	0.03	0.06	0.09	0.09	0.07
Er	0.27	0.07	0.14	0.56	0.10	0.03	0.05	0.08	0.17	0.27	0.27	0.19
Tm	0.03	0.01	0.02	0.08	0.01	0.00	0.01	0.01	0.02	0.04	0.04	0.02
Yb	0.21	0.05	0.10	0.52	0.08	0.02	0.04	0.07	0.15	0.24	0.24	0.16
Lu	0.03	0.01	0.02	0.08	0.01	<0.01	0.01	0.01	0.02	0.04	0.04	0.02
ΣREE	25.1	7.2	14.7	27.0	10.6	1.9	2.2	4.3	11.6	15.7	15.9	12.7
Ce/Ce*	1.55	1.58	1.57	1.25	1.64	0.55	0.45	0.78	0.97	0.99	1.01	0.98
Eu/Eu*	1.59	2.14	2.10	1.28	3.78	1.23	0.94	1.1	5.08	4.02	4.46	5.19
Pr/Pr*	0.79	0.79	0.77	0.83	0.75	1.14	1.24	1.12	0.92	0.94	0.90	0.91
Mo	0.58	0.50	0.55	1.19	0.52	0.32	n.d	n.d	0.36	0.32	0.25	0.18
U	2.88	1.41	1.96	8.62	2.92	3.39	n.d	n.d	1.95	0.60	0.30	1.59

n.d: no data.
* (a) and (b): data from Birgel et al. (2011) by 5% HNO_3 dissolution.

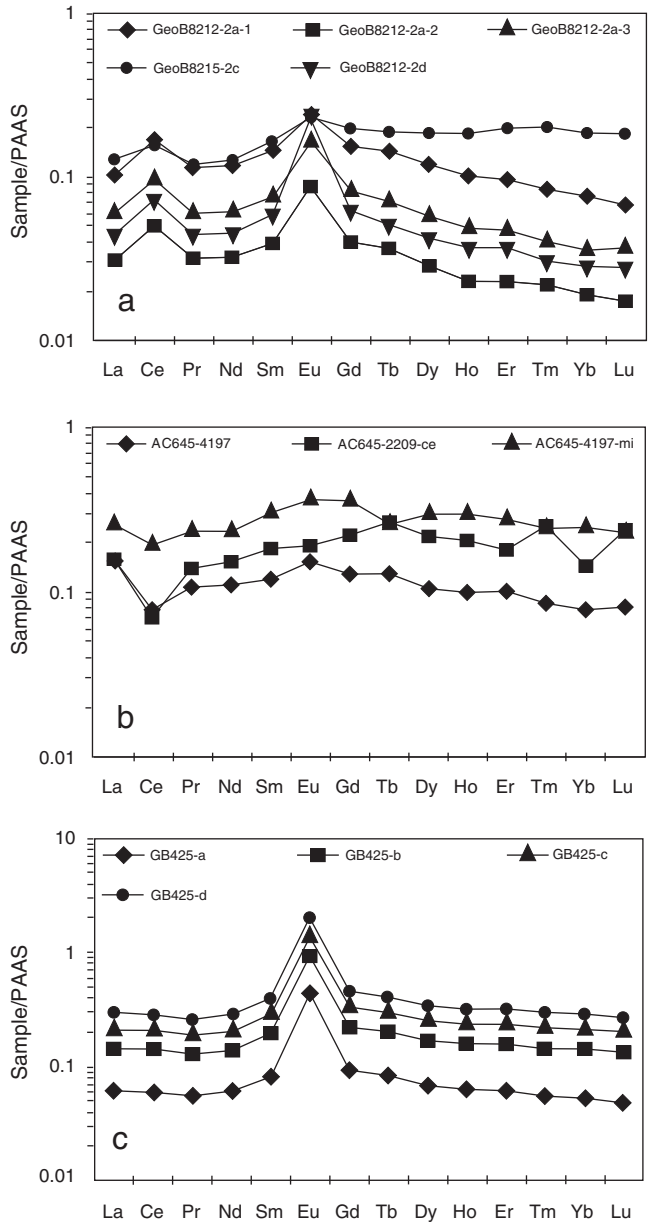

Fig. 2. PAAS-normalized REE patterns of authigenic carbonates. (a) Congo Fan carbonate samples; (b) AC645 carbonate samples, AC645-2209-ce and AC645-4197-mi: data from Birgel et al. (2011); (c) GB425 carbonate samples.

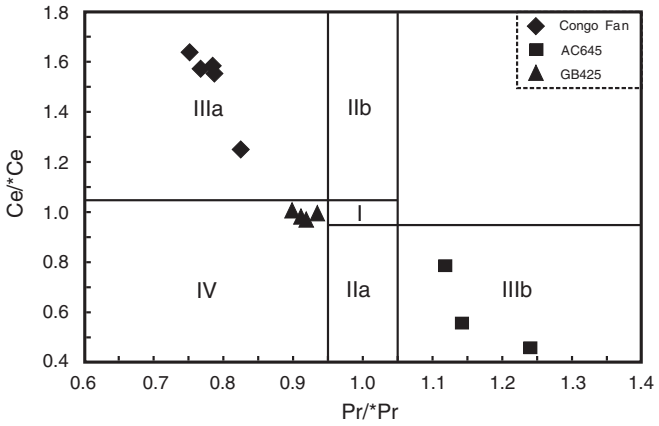

Fig. 3. $(Ce/Ce^*)_{SN}$ vs. $(Pr/Pr^*)_{SN}$ diagram after Bau and Dulski (1996) and Shields et al. (2004). Field I: no anomaly; field IIa: positive La anomaly produces an apparent negative Ce anomaly; field IIb: a negative La anomaly causes an apparent positive Ce anomaly; field IIIa: real positive Ce anomaly; field IIIb: real negative Ce anomaly; field IV: positive La anomaly disguises a positive Ce anomaly.

5. Discussion

5.1. Molybdenum, uranium, and rare earth element geochemistry

5.1.1. CF seep carbonates

Molybdenum behaves conservatively in oxic conditions, existing as molybdate. However, the presence of hydrogen sulfide tends to facilitate conversion of molybdate to thiomolybdates, and the latter is eventually incorporated by iron sulfide phases or sulfidized organic matter, resulting in anomalous enrichment of Mo in sediments in euxinic basins (Helz et al., 1996; Tribovillard et al., 2006; Neubert et al., 2008; Algeo and Tribovillard, 2009; Helz et al., 2011; Nägler et al., 2011; Kowalski et al., 2013). Anomalous high Mo concentrations (from 1.7 ppm to 28.3 ppm) were observed in seep sediments from the Nankai Trough, believed to reflect the formation of iron sulfide after hydrogen sulfide was generated during AOM (Sato et al., 2012). In seep sediment cores recovered from the Krishna–Godavari basin, the maximum Mo concentrations of the paleo-sulfate methane transition zone reached even 37 ppm, and the marked Mo anomalies were again attributed to sulfide mineral formation after hydrogen sulfide

present in GB425 samples (mean 0.9 ppm). Samples of CF and GB425 also revealed high Ba concentrations (see Appendix 2).

The Mo_{EF} relative to PAAS of CF, GB425, and AC645 carbonates decreases as the Mo concentrations drop except for the sub-samples of AC645 highlighted by a circle in Fig. 4. The sub-samples highlighted by the circle yielded low Mo concentrations (below 2 ppm), while the remarkably high Mo_{EF} resulted from extremely low Al contents of the pure aragonite sampled. Regarding the enrichment factors after normalization to Crust (McLennan, 2001), Mo, As, and Sb show major enrichment in GB425 samples (most of Mo_{EF} near to 10; almost all Sb_{EF} and As_{EF} above 10). In contrast, the enrichment factors of U, Ni, Co, Pb, and Zn only occasionally exceed 10 with most factors below 10 and the factors of Cr_{EF}, Cu_{EF}, Th_{EF}, and V_{EF} all near to 3, illustrating that these trace elements are not significantly enriched in GB425 samples (Table 3).

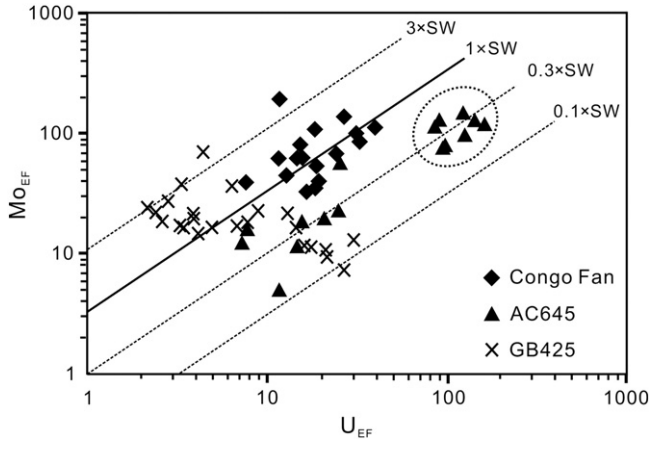

Fig. 4. Enrichment factors (EF); Mo_{EF} vs. U_{EF} for authigenic carbonates in this study (modified from Algeo and Tribovillard (2009)). $(Mo/U)_{SW} = 3.1$. EF are calculated as follows: $X_{EF} = [(X/Al)_{sample}/(X/Al)_{PAAS}]$, samples are normalized using the Post Archean Australian Shale (PAAS) composition (Taylor and McLennan, 1985). Note the triangles in the circle of AC645 samples, remarkably high Mo_{EF} and U_{EF} of these sub-samples result from the extremely low Al contents (all Al_2O_3 contents below 0.33%).

Table 3
Enrichment-factor, Fe/Al and Mn/Al ratios of GB425 authigenic carbonates.

Sample ID	Mo_{EF}	As_{EF}	Sb_{EF}	U_{EF}	Ni_{EF}	Co_{EF}	Cr_{EF}	Cu_{EF}	Pb_{EF}	Th_{EF}	V_{EF}	Zn_{EF}	Fe/Al	Mn/Al
GB425-1	9.1	106.6	n.d	6.0	7.4	2.9	3.7	3.2	1.7	1.2	3.6	5.5	1.55	0.09
GB425-2	14.3	223.8	n.d	2.5	6.7	4.0	2.0	1.1	1.9	1.3	4.4	5.5	2.12	0.14
GB425-3	12.2	74.2	n.d	8.0	8.4	3.2	2.3	0.8	1.8	1.2	3.1	10.4	1.40	0.12
GB425-4	6.1	115.1	n.d	15.8	5.7	2.4	2.3	0.8	1.9	1.3	3.2	5.9	1.40	0.06
GB425-5	19.7	499.6	n.d	3.1	6.5	5.3	1.9	0.9	13.6	1.1	6.0	6.3	3.47	0.19
GB425-6	8.8	168.4	n.d	4.4	7.8	3.8	4.0	2.8	1.9	1.4	4.2	4.8	1.90	0.15
GB425-7	8.7	125.8	n.d	13.2	6.1	2.5	2.3	1.4	1.5	1.3	3.7	8.5	1.49	0.08
GB425-8	10.0	99.5	n.d	2.4	7.8	4.0	5.9	2.0	1.6	1.3	3.1	3.7	1.14	0.09
GB425-9	12.8	91.5	n.d	1.9	5.1	2.2	2.7	3.4	33.5	1.4	3.3	6.4	1.31	0.04
GB425-10	19.5	118.7	n.d	5.7	13.0	3.5	7.8	2.2	1.8	1.3	4.2	5.5	1.62	0.10
GB425-11	10.4	130.0	n.d	3.5	9.6	3.5	4.2	1.2	1.5	1.4	4.4	4.0	1.79	0.16
GB425-12	11.6	116.7	n.d	2.2	5.4	2.4	2.3	1.8	1.6	1.3	4.1	4.7	1.51	0.06
GB425-13	8.9	39.2	n.d	3.1	7.4	3.1	3.2	1.3	1.2	1.2	3.4	3.8	1.60	0.13
GB425-14	36.9	57.6	n.d	4.0	10.3	13.9	6.4	1.6	2.4	1.5	3.3	5.1	1.27	0.41
GB425-15	4.0	38.1	9.8	24.4	4.7	1.9	1.8	4.4	1.2	1.0	2.7	3.0	1.07	0.03
GB425-16	7.9	40.7	23.8	3.7	4.0	3.8	1.6	4.3	1.3	1.0	2.4	4.3	0.95	0.15
GB425-17	5.8	36.8	17.7	19.4	4.4	2.6	1.5	3.9	1.4	1.0	2.4	3.3	0.98	0.07
GB425-18	10.0	51.6	12.7	7.1	6.2	2.7	1.6	2.7	1.5	0.9	3.0	2.4	1.13	0.09
GB425-19	5.1	48.9	11.6	19.8	3.5	1.6	1.5	3.0	1.2	1.0	2.8	3.9	1.14	0.03
GB425-20	6.4	31.0	19.7	14.7	4.5	2.3	1.9	2.8	1.4	1.0	2.7	2.5	0.93	0.07
GB425-21	11.6	34.3	27.0	11.7	6.3	3.8	1.8	2.8	1.5	1.0	2.9	3.1	1.18	0.15
GB425-22	7.0	59.4	39.1	27.5	6.6	2.4	1.7	3.5	1.7	1.0	3.2	3.4	1.14	0.06
GB425-23	9.3	70.1	27.6	3.0	8.2	2.2	4.7	3.2	6.8	1.0	2.7	2.8	1.29	0.11
GB425-24	11.7	371.2	49.0	3.5	6.1	4.2	1.6	2.7	1.9	1.0	5.5	4.0	2.98	0.17

Note: $X_{EF} = [(X / Al)_{sample} / (X / Al)_{Crust}]$, samples are normalized using the Earth's upper crust (crust) composition (McLennan, 2001). n.d: no data.

was produced by intense AOM (Peketi et al., 2012). Likewise, similar Mo anomalies were observed in this study in CF seep carbonates with Mo concentrations commonly above 10 ppm — significantly exceeding crustal average (1–2 ppm; Taylor and McLennan, 1985). Pyrite framboids are particularly abundant in CF carbonates (Feng et al., 2010a). Thus, it seems likely that the Mo enrichment in CF seep carbonate is linked to iron sulfide phases, representing a product of hydrogen sulfide formation during AOM. In fact, carbonate sediments and rocks (>30% $CaCO_3$) generally contain an average Mo concentration of 1.1 ppm, and Mo concentration of pure carbonate is close to 0.1 ppm (Morford and Emerson, 1999; Voegelin et al., 2009). Molybdenum concentration of authigenic carbonate phases in the carbonate rocks (dissolution in 5% acetic acid solutions) of this study averages 0.5 ppm (Table 2), a concentration between the range of Mo concentrations in carbonate sediments and rocks on the one hand and pure carbonate minerals on the other hand. Consequently, it seems most likely that iron sulfides are the main Mo-bearing phases considering the low Mo concentrations in authigenic carbonates and detrital phases. The $(Mo/U)_{EF}$ ratios of CF carbonates equal or exceed ratios in seawater. Suboxic sediments typically reveal low $(Mo/U)_{EF}$ ratios, whereas euxinic sediments typically exhibit much higher ratios (e.g., Algeo and Tribovillard, 2009). Such patterns together with extremely high Mo contents (Fig. 4) indicate that CF seep carbonates precipitated in a sulfidic environment. The high concentrations of U and ΣREE present in CF carbonates agree with anoxic conditions. Furthermore, CF carbonates exhibit high U_{EF} and positive Ce anomalies (Figs. 2 and 4), which also point to strictly anoxic conditions during carbonate formation.

If sulfidic conditions are restricted to pore waters, sediment Mo concentrations average ~10 ppm and rarely exceed 25 ppm (Scott and Lyons, 2012). Conversely, in euxinic environments where hydrogen sulfide is present in the water column, Mo concentrations exceed 60 ppm and can reach 100 s ppm in the sediments below euxinic water columns (Scott and Lyons, 2012). Numerous studies on modern seeps and modern and ancient seep carbonates revealed that seepage activity varies episodically (Aharon et al., 1997; Roberts and Carney, 1997; Tryon et al., 1999; Teichert et al., 2003; Bayon et al., 2009; Feng et al., 2010b; Bian et al., 2013; Tong et al., 2013). Based on this variability, AOM-derived hydrogen sulfide may even build up in the uppermost sediments or may even seep into the water column. This circumstance explains the distribution of Mo in seep sediments and carbonates observed in this and other studies (cf. Peketi et al., 2012; Sato et al., 2012). To sum up, CF carbonates formed under strongly reducing conditions as revealed by positive Ce anomalies. The observed trace element patterns suggest that hydrogen sulfide build up to high concentration in surface-near sediments and may even have seeped into the water column episodically.

5.1.2. AC645 seep carbonates

The AC645 carbonates yielded Mo concentrations in the range of 0.8 ppm to 2.9 ppm with an average of 1.6 ppm (close to the crustal average: 1–2 ppm; Taylor and McLennan, 1985), reflecting the lack of Mo enrichment in AC645 carbonates. The partially high Mo_{EF} of AC645 carbonates should be considered with caution in view of the extremely low Al contents of the AC645 aragonites that yielded the highest enrichment factors (Fig. 4). Three drawbacks may occur in the application of Al normalization: (1) a relative excess of Al compared to overall detrital input; (2) the reference values of normalized elements are not necessarily representative for the sediments in the study area; and (3) the coefficient of variation (e.g. standard deviation divided by the mean) of the Al concentration is large compared to that of the trace element concentration (Van der Weijden, 2002; Tribovillard et al., 2006 and references therein). The spurious high Mo_{EF} in AC645 carbonates is best explained by the last scenario based on the much higher coefficient of variation of the Al concentration than that of the Mo concentration. The absence of euxinic conditions is in fact confirmed by low $(Mo/U)_{EF}$ ratios (about $0.3 \times (Mo/U)_{sw}$; Fig. 4). Thus, the pattern of authigenic U–Mo covariation with low $(Mo/U)_{EF}$ ratios suggests that suboxic–anoxic rather than sulfidic conditions were dominant during the formation of AC645 carbonates.

The AC645 carbonates are composed almost entirely of aragonite, pointing to a formation environment close to the seafloor that was characterized by high alkalinity and sulfate concentrations (Burton, 1993; Luff and Wallmann, 2003; Peckmann et al., 2009). If the conditions during carbonate formation would have been characterized by the presence of hydrogen sulfide produced by sulfate-dependent AOM, molybdate would have been converted to thiomolybdates (Helz et al., 1996, 2011), leading to Mo enrichment. The fact that no substantial

Mo enrichment was observed in AC645 carbonates agrees with the absence of high sulfide concentrations in the surface sediments. The negative Ce anomalies observed for AC645 carbonates may result from high pore water alkalinity in the presence of organic matter (cf. Pourret et al., 2008; Kim et al., 2012). However, this explanation cannot account for the absence of Mo enrichment. Intermittent oxygenation is an alternative explanation for the negative Ce anomalies, the presence of biomarkers of aerobic methanotrophic bacteria (cf. Birgel et al., 2011), and the absence of Mo enrichment in AC645 carbonates. Likewise, seafloor observations suggested that the downward flow of oxic seawater into the anoxic sediment at some seeps is significant (Solomon et al., 2008). It seems feasible that the downward flow of oxic seawater oxidizes some of the AOM-generated hydrogen sulfide, keeping sulfide concentration at a level that is too low to allow for Mo enrichment.

5.1.3. GB425 seep carbonates

At the GB425 mud volcano site, seeping fluids are typified by an anoxic hypersaline brine supersaturated with methane, and hydrogen sulfide was found to be barely detectable (MacDonald et al., 2000; Joye et al., 2005). Observations over eight years documented substantial temperature variations and discontinuous fluid discharge (MacDonald et al., 2000; Joye et al., 2005). The average Mo concentrations and Mo_{EF} in GB425 samples fall between the range of those in the CF and AC645 samples (Fig. 4). However, the $(Mo/U)_{EF}$ ratios in GB425 samples, varying from $0.1 \times (Mo/U)_{SW}$ to $3 \times (Mo/U)_{SW}$, are remarkably different from that of the CF and AC645 samples. The varying $(Mo/U)_{EF}$ ratios are best explained by changing redox conditions during the formation of GB425 carbonates possibly induced by changes in seepage flux (cf. Feng et al., 2009a,b; Birgel et al., 2011). On the other hand, the GB425 samples exhibit MREE (Sm, Gd, Tb, Dy) enrichment, which is a typical feature of pore waters of the iron reduction zone (Haley et al., 2004; Bayon et al., 2011; Kim et al., 2012). Considering the MREE enrichment, the absence of Ce anomalies, and Mo–U covariation patterns, it seems likely that GB425 carbonates precipitated in suboxic to anoxic sediments near to the iron reduction zone.

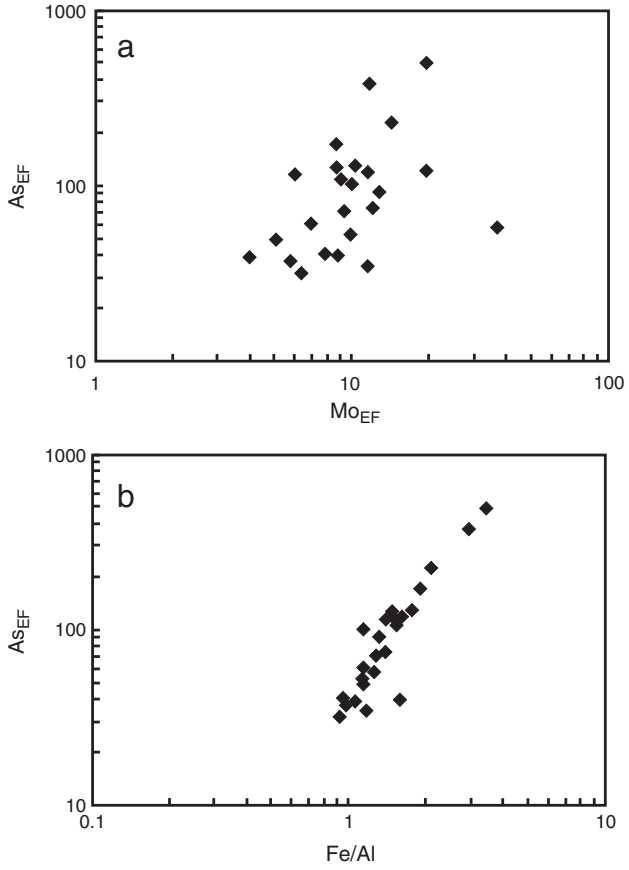

Fig. 5. Arsenic (As) patterns; (a) As_{EF} vs. Mo_{EF}, (b) As_{EF} vs. Fe/Al ratios for GB425 carbonates. Enrichment factors (EF) are calculated as following: $X_{EF} = [(X / Al)_{sample} / (X / Al)_{Crust}]$, samples are normalized using the Earth's upper crust (crust) composition (McLennan, 2001).

5.2. Molybdenum, arsenic, and antimony enrichments of GB425 samples

Recently, enrichments of Mo, As, and Sb have been reported in cold-seep fluids and sediments of mud volcanos, ancient seep carbonates, and hydrocarbon-derived ferromanganese nodules (Nath et al., 2008; Cangemi et al., 2010; González et al., 2012; Tribovillard et al., 2013). In this study, similar enrichments of Mo, As, and Sb are observed in GB425 seep carbonates and, surprisingly, As enrichment were even found to exceed those of Mo (Fig. 5a). Major element contents (Ca, Al, Fe, Mn) and Mo concentrations in GB425 samples are similar to those of Jurassic seep carbonates, but As and Sb concentrations are higher than those in the ancient limestones (cf. Tribovillard et al., 2013). The other trace metals do not show significant enrichment in GB425 seep carbonates, although some elements (e.g. U, Ni) have enrichment factors occasionally exceeding 10 (Table 3). With respect to the mechanism of Mo, As, and Sb enrichment, two hypotheses have been brought forward: (1) the trace metals were carried to the surface sediments by ascending seep fluids, resulting in trace-metal enrichment in the shallow pore fluid and sediments (Nath et al., 2008; Cangemi et al., 2010); (2) the trace metals were predominantly derived from the seawater, scavenged by iron and manganese oxyhydroxides in the water column, and then transferred to the surface sediments (Tribovillard et al., 2013).

At GB425, the seeping brines were found to result from halite dissolution and contain no sulfate (Joye et al., 2005; Joye and Samarkin, 2009). If the chloride-rich ascending brine carries Mo, As, and Sb to the surface sediments, the brine would also simultaneously capture other elements in the stable form of chlorides (such as Cu, Ni and Zn) and it would easily remobilize U, resulting in enrichment of all these elements in the shallow sediments (cf. Tribovillard et al., 2013 and references therein). However, the above scenario is inconsistent with the fact that only Mo, As, and Sb enrichments were recognized in GB425 carbonates.

It has been established that manganese oxyhydroxides are the main carriers of Mo, transporting this element from the seawater to the sediment by the so-called particulate shuttle process (Tribovillard et al., 2006; Chaillou et al., 2008; Dellwig et al., 2010; Scott and Lyons, 2012; Tribovillard et al., 2013). A similar process probably applies to the redistribution of As and Sb by iron oxyhydroxides (Cutter et al., 2001; Chaillou et al., 2008; Böning et al., 2009; Wang et al., 2012; Tribovillard et al., 2013). Because other elements are known to be unaffected by the particulate shuttle process (e.g. Tribovillard et al., 2013), only Mo, As, and Sb enrichments are found in seep sediments and carbonates. But why then are seep sediments enriched in these elements, although the particulate shuttle process is obviously not restricted to the water column above seeps? It seems likely that the enhanced formation of AOM-induced sulfide minerals at seeps captures much of these chalcophile elements, avoiding subsequent loss of Mo, As, and Sb to the water column after reduction of the manganese and iron oxyhydroxides in anoxic sediments (cf. Tribovillard et al., 2013). In addition, anomalous enrichment of Mo, As, and Sb was frequently observed in ferromanganese nodules and crusts in normal marine environments (Calvert and Price, 1977; Koschinsky and Hein, 2003; Dekov et al., 2007). In these cases, the elements were directly derived from seawater, indicating that seawater without other sources (e.g. ascending fluids) has the potential to supply enough trace elements to

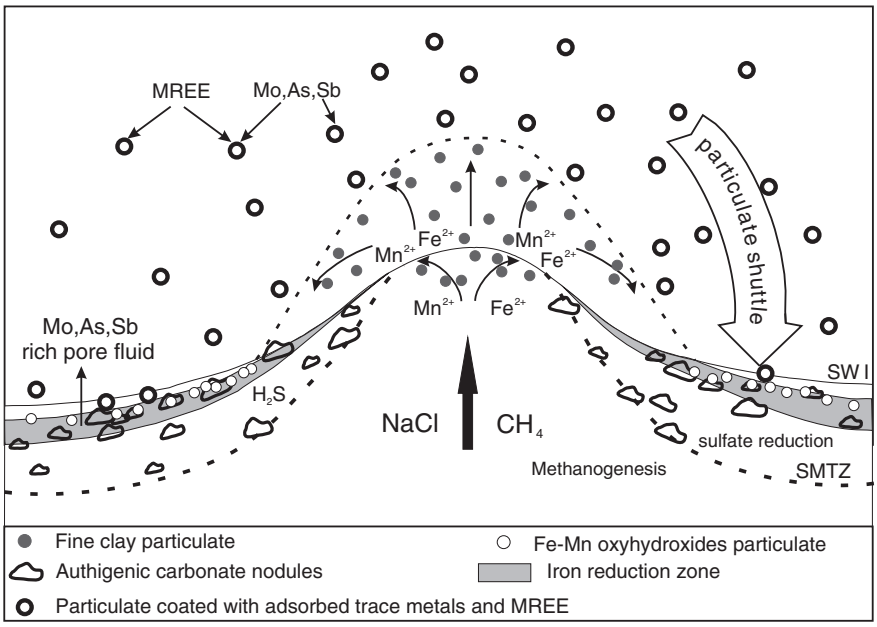

Fig. 6. Schematic diagram illustrating the adsorption and transportation process of Mo, As, and Sb and MREE by iron and manganese oxyhydroxide particulates in and above the mud volcano of GB425. The particulate shuttle process favors: (1) the adsorption of these trace metals to aggregates of iron and manganese oxyhydroxides in the water column; (2) their transport to the sediment; (3) their release upon the reduction of oxyhydroxides in suboxic sediments; and (4) their immobilization due to incorporation into authigenic minerals resulting from the anaerobic oxidation of methane at seeps. The reasoning that MREE are preferentially adsorbed to oxyhydroxides is based on Bayon et al. (2011). SWI: sediment–water interface, SMTZ: sulfate methane transition zone.

generate the observed anomalies. Finally, the GB425 carbonates contain high concentrations of Fe and Mn, confirming that particulate shuttle processes are feasible. In particular, the enrichment factor of As (As_{EF}) correlates well with the authigenic fraction of Fe (Fe/Al) (Fig. 5b), confirming that iron oxyhydroxides may play a critical role in the development of Mo, As, and Sb enrichments, although additional input from ascending fluids cannot be ruled out.

Above the pockmark field of the Niger Delta margin, methane plumes were found to rise up to about 100 m above the seafloor (Bayon et al., 2011). Within these plumes iron and manganese oxyhydroxides occur (Bayon et al., 2011). It was further concluded that iron and manganese oxyhydroxides actively scavenge REE, especially MREE (Bayon et al., 2011). The same conclusion is believed to apply for Mo, As, and Sb (Tribovillard et al., 2013). At the GB425 mud volcano, the methane plume reached >200 m above the seafloor (Joye et al., 2005). The abundance of suspended particulates in the GB425 brine was found to provide an iron oxide source to fuel sulfide oxidation (Joye et al., 2005). It seems consequently feasible that the suspended particulates and the high Fe^{2+} concentrations in the mud volcano fluids facilitate the precipitation of iron and manganese oxyhydroxides within the methane plume (see Fig. 6 for a schematic diagram). In this scenario, the formation of iron and manganese oxyhydroxides results in preferential removal of dissolved Mo, As, Sb, and MREE from the surrounding seawater. Subsequently the iron and manganese particulates sink to the sediment–water interface and become exposed to the iron reduction zone upon ongoing sedimentation. After the iron and manganese particulates are reduced, Mo, As, Sb, and MREE are released into the pore water, leading to the enrichment of these elements in the proximity of the iron reduction zone. The released elements can either return back to the water column or become incorporated into authigenic sulfides or even carbonates (Sato et al., 2012; Tribovillard et al., 2013, and references therein).

6. Conclusions

Authigenic carbonates from cold hydrocarbon seeps from the AC645 and GB425 sites of the Gulf of Mexico and from pockmarks on the Congo Fan are characterized by negative, no, and positive Ce anomalies, respectively. Moreover, the highest overall contents of ΣREE and Mo as well as the highest ratios of $(Mo/U)_{auth}$ were found in Congo Fan seep carbonates. Carbonates from AC645 were found to have the lowest ΣREE and Mo contents as well as the lowest $(Mo/U)_{auth}$ ratios. In this context, the formation environments of authigenic carbonates reflect a trend toward more reducing conditions from AC645 over GB425 to the Congo Fan seeps. The Congo Fan carbonates formed under sulfidic conditions and high concentrations of AOM-derived hydrogen sulfide build up in the uppermost sediments, possibly even leading to episodic release of hydrogen sulfide into the water column. No substantial Mo enrichment and low $(Mo/U)_{auth}$ ratios in the AC645 carbonates suggest that the observed negative Ce anomalies reflect intermittent oxygenation. Variable $(Mo/U)_{auth}$ ratios in samples from the GB425 site were apparently caused by episodic changes of the seepage intensity. The enrichment of Mo, As, and Sb in GB425 carbonates is interpreted to reflect an efficient particulate shuttle process. Similar processes and scenarios may apply to other modern and fossil cold seep sites.

Acknowledgments

Samples from the Gulf of Mexico sites were collected during cruises sponsored by the BOEM and the NOAA. Dr. S.B. Joye (University of Georgia) is acknowledged for providing GB425 samples. We express our sincere appreciation to Dr. G. Bohrmann (University of Bremen) for providing the Congo Fan samples. We thank Dr. L. Qi (Institute of Geochemistry, CAS) for helping with the analysis of REE, major, and trace elements. We thank journal editor Dr. M.E. Böttcher and two anonymous reviewers for constructive comments, which considerably improved the quality of the manuscript. This study was partially supported by the NSF of China (Grants: 91228206 and 41373085), the "Hundred Talents Program" of CAS, and the LSU Boyd Professionship. This is contribution No. IS-1859 from GIGCAS.

Appendix 1. Major element contents (wt.%) of bulk authigenic carbonates

Sample ID	MgO	Al_2O_3	P_2O_5	CaO	TiO_2	MnO	Fe_2O_3
CF-1	5.74	1.50	0.03	36.8	0.08	0.01	1.46
CF-2	0.73	1.23	0.01	39.3	0.07	0.01	1.43
CF-3	4.41	1.23	0.02	38.5	0.06	0.01	1.43
CF-4	1.06	1.24	0.01	37.9	0.07	0.01	1.31
CF-5	2.15	1.09	0.01	40.7	0.06	0.01	1.27
CF-6	0.76	1.02	0.02	39.5	0.07	0.00	1.34
CF-7	4.17	1.46	0.03	37.7	0.08	0.01	1.42
CF-8	6.85	1.63	0.04	36.9	0.08	0.01	2.06
CF-9	4.77	1.91	0.06	35.2	0.11	0.01	2.27
CF-10	4.93	1.87	0.06	36.3	0.11	0.02	2.06
CF-11	4.00	1.79	0.05	38.2	0.10	0.03	2.17
CF-12	4.70	1.82	0.05	35.3	0.10	0.01	1.96
CF-13	4.80	1.82	0.04	39.4	0.11	0.03	1.90
CF-14	2.63	1.18	0.02	39.5	0.06	0.01	1.35
CF-15	2.13	1.36	0.03	40.9	0.07	0.01	1.34
CF-16	4.08	1.42	0.02	42.5	0.08	0.01	1.74
CF-17	4.00	1.43	0.01	40.7	0.08	0.01	1.41
AC645-1	0.14	0.31	0.02	43.7	0.02	0.01	0.95
AC645-2	0.14	0.33	0.02	44.2	0.02	0.01	0.92
AC645-3	0.13	0.31	0.01	41.8	0.02	0.01	0.87
AC645-4	0.10	0.19	0.02	42.2	0.01	0.01	0.84
AC645-5	0.11	0.29	0.02	42.5	0.02	0.01	0.91
AC645-6	0.10	0.19	0.01	42.5	0.01	0.01	1.17
AC645-7	0.09	0.18	0.01	43.8	0.01	0.01	0.84
AC645-8	1.77	2.10	0.04	39.2	0.14	0.03	2.23
AC645-9	0.11	0.29	0.02	41.4	0.02	0.01	0.88
AC645-10	0.55	1.53	0.03	37.2	0.09	0.02	1.34
AC645-11	1.16	2.84	0.04	35.2	0.16	0.02	1.89
AC645-12	1.37	1.30	0.06	41.6	0.07	0.01	1.23
AC645-13	0.59	0.92	0.03	40.1	0.05	0.01	1.18
AC645-14	1.01	2.21	0.04	37.5	0.12	0.01	1.57
AC645-15	1.49	2.34	0.05	39.1	0.14	0.02	1.73
AC645-16	1.04	1.84	0.03	38.0	0.12	0.01	1.45
GB425-1	1.78	2.20	0.08	39.1	0.14	0.13	2.58
GB425-2	1.61	2.31	0.16	37.0	0.16	0.23	3.71
GB425-3	1.97	1.77	0.08	43.8	0.11	0.15	1.88
GB425-4	1.74	2.40	0.12	37.9	0.16	0.10	2.54
GB425-5	1.82	2.84	0.32	35.3	0.19	0.36	7.44
GB425-6	1.41	1.78	0.09	34.1	0.12	0.18	2.56
GB425-7	1.57	2.00	0.08	35.6	0.13	0.11	2.25
GB425-8	1.73	2.44	0.07	33.1	0.16	0.15	2.11
GB425-9	1.54	2.56	0.10	27.8	0.19	0.07	2.53
GB425-10	1.55	1.83	0.06	34.0	0.12	0.13	2.25
GB425-11	1.68	1.81	0.08	39.3	0.12	0.20	2.44
GB425-12	1.81	2.51	0.10	33.1	0.17	0.10	2.87
GB425-13	1.81	2.16	0.08	37.1	0.14	0.19	2.61
GB425-14	1.83	2.10	0.08	39.1	0.14	0.59	2.02
GB425-15	1.93	2.56	0.09	39.4	0.17	0.06	2.07
GB425-16	1.67	3.09	0.10	34.9	0.20	0.32	2.22
GB425-17	1.89	2.87	0.10	37.5	0.19	0.14	2.12
GB425-18	1.93	2.94	0.10	41.2	0.19	0.19	2.51
GB425-19	1.96	3.34	0.10	38.7	0.19	0.07	2.89
GB425-20	1.83	3.27	0.11	39.5	0.20	0.17	2.30
GB425-21	1.69	2.22	0.10	45.8	0.15	0.22	1.98
GB425-22	2.33	2.60	0.10	42.3	0.17	0.12	2.24
GB425-23	1.75	2.72	0.11	42.2	0.18	0.20	2.66
GB425-24	1.83	2.87	0.12	38.1	0.19	0.33	6.46

Appendix 2. Trace element contents (ppm) of bulk authigenic carbonates

Sample ID	V	Cr	Co	Ni	Cu	Zn	Sr	Zr	Mo	Sb	Ba	Pb	Th	U	As
CF-1	20.3	15.7	4.6	33.1	7.6	43.6	2121	12.0	14.9	n.d	705	4.5	2.5	2.9	3.9
CF-2	17.4	34.5	4.0	47.2	5.9	34.2	7315	11.0	4.0	n.d	567	4.5	1.2	2.4	4.5
CF-3	17.1	14.6	4.0	54.0	2.3	27.3	3794	11.6	2.8	n.d	972	2.5	1.6	2.6	3.5
CF-4	19.4	15.2	3.7	30.6	3.7	23.8	7208	12.3	5.2	n.d	609	2.9	1.3	3.2	3.9
CF-5	19.5	21.6	3.2	32.9	1.3	43.5	6301	11.3	4.0	n.d	990	3.8	2.9	4.5	2.1
CF-6	16.8	38.4	3.5	42.2	4.0	32.4	7703	12.3	3.3	n.d	578	2.2	1.1	2.5	1.7
CF-7	21.1	20.4	4.0	35.9	5.8	39.2	3723	13.9	3.0	n.d	773	3.1	1.2	1.8	4.9
CF-8	26.7	20.2	4.2	33.9	6.6	52.9	1672	12.9	2.9	n.d	563	3.3	2.5	4.5	4.6
CF-9	41.4	24.9	5.3	38.2	7.5	36.4	886	18.8	10.7	n.d	600	3.8	1.9	5.9	10.3
CF-10	40.0	26.0	6.1	33.8	6.2	76.5	889	19.0	9.9	n.d	454	4.4	1.8	9.6	9.3
CF-11	43.5	22.6	6.1	39.7	15.7	105.2	1756	18.9	10.6	n.d	515	5.5	2.6	12.0	12.5
CF-12	41.3	24.3	5.8	37.3	6.9	29.1	946	17.4	13.0	n.d	608	3.3	2.0	8.2	9.0
CF-13	42.5	28.9	5.5	44.4	8.5	65.4	1260	18.4	8.0	n.d	455	4.5	1.9	9.8	7.9
CF-14	17.0	15.8	4.2	33.4	8.5	86.6	6079	13.0	3.3	n.d	4769	11.9	1.1	3.7	3.6
CF-15	19.6	17.7	4.3	34.0	5.1	65.3	6083	22.6	4.4	n.d	894	3.3	1.4	3.5	5.5
CF-16	19.4	20.6	4.0	36.6	6.0	59.6	4092	13.3	2.6	n.d	897	2.4	1.6	4.4	1.7
CF-17	18.1	16.9	4.1	33.1	7.0	40.9	5011	14.9	3.0	n.d	7355	3.9	1.3	4.6	n.d
AC645-1	12.1	16.1	2.9	35.2	5.1	42.9	6540	4.6	2.2	n.d	31	0.6	0.2	4.8	0.5
AC645-2	13.9	14.9	2.9	34.3	3.1	26.4	6643	4.5	2.0	n.d	25	0.4	0.2	4.8	2.0
AC645-3	16.2	11.5	2.7	35.0	6.9	25.0	6504	4.3	2.5	n.d	27	0.9	0.3	6.5	0.7
AC645-4	9.9	11.7	2.4	32.9	3.5	24.3	6406	5.1	1.0	n.d	20	0.4	0.2	3.9	0.6
AC645-5	12.1	11.4	2.7	31.0	5.1	13.5	6455	3.8	1.2	n.d	24	1.1	0.2	4.5	0.3
AC645-6	13.6	11.4	2.6	35.3	9.6	23.6	6556	2.8	1.2	n.d	28	0.6	0.2	5.0	0.4
AC645-7	12.0	8.6	2.8	34.9	4.5	22.6	6655	2.5	1.3	n.d	23	0.5	0.2	4.4	0.3
AC645-8	13.1	14.8	2.8	52.3	3.5	36.6	6645	35.9	1.3	n.d	25	0.6	0.3	5.0	0.1
AC645-9	13.7	12.4	2.8	36.1	6.4	22.1	6637	3.4	1.2	n.d	66	2.9	0.2	4.8	0.9
AC645-10	39.3	27.9	5.2	38.0	9.3	41.3	8272	27.9	1.7	n.d	112	3.0	1.3	5.2	3.2
AC645-11	59.6	33.6	8.0	38.6	12.9	44.1	5236	32.2	0.8	n.d	103	4.5	2.0	5.4	6.1
AC645-12	30.1	32.5	4.3	45.7	12.9	49.8	5848	17.3	1.6	n.d	62	3.0	0.9	5.4	2.4
AC645-13	19.1	108.9	3.4	80.8	9.8	37.5	6088	9.2	2.9	n.d	56	1.9	0.7	3.9	2.8
AC645-14	44.0	23.4	4.9	34.3	10.0	38.7	7717	25.5	1.5	n.d	129	3.6	1.7	2.6	3.8
AC645-15	56.3	31.9	5.5	33.6	15.2	64.2	4558	33.5	1.9	n.d	115	9.4	2.2	3.0	7.2
AC645-16	46.3	25.9	5.5	35.9	11.0	36.7	6863	24.6	1.9	n.d	105	3.2	1.6	4.8	8.1
GB425-1	55.8	44.2	7.2	47.3	11.7	56.7	792	52.7	2.0	n.d	5693	4.3	1.9	2.5	23.2
GB425-2	71.8	25.7	10.4	45.1	4.2	59.4	599	43.8	3.3	n.d	243	5.0	2.1	1.1	51.1
GB425-3	38.7	22.7	6.3	43.1	2.3	85.9	786	40.2	2.1	n.d	348	3.5	1.5	2.6	13.0
GB425-4	54.3	30.2	6.4	39.4	3.0	66.0	822	57.7	1.4	n.d	428	5.2	2.2	7.0	27.2
GB425-5	120.7	29.4	16.7	53.4	4.3	83.6	625	69.2	5.5	n.d	237	43.0	2.2	1.6	140.0
GB425-6	52.0	38.4	7.5	39.9	8.2	39.7	588	40.5	1.5	n.d	232	3.7	1.7	1.5	29.5
GB425-7	52.5	25.7	5.7	35.7	4.6	80.0	825	47.5	1.7	n.d	6633	3.4	1.8	4.9	24.9
GB425-8	53.6	78.6	11.1	55.2	8.0	42.7	1171	51.3	2.4	n.d	14369	4.5	2.2	1.1	24.0
GB425-9	60.1	37.3	6.2	37.5	14.1	76.1	2197	59.5	3.2	n.d	61475	95.9	2.6	0.9	23.1
GB425-10	54.7	77.9	7.3	69.3	6.8	46.8	1338	37.9	3.5	n.d	16742	3.6	1.7	1.9	21.5
GB425-11	56.5	41.4	7.2	50.4	3.6	34.1	647	35.9	1.9	n.d	292	3.0	1.7	1.2	23.2
GB425-12	72.9	31.7	6.8	39.3	7.3	54.6	1382	48.2	2.9	n.d	20362	4.6	2.4	1.0	29.0
GB425-13	51.9	37.9	7.6	46.5	4.5	38.7	924	37.4	1.9	n.d	9817	2.9	1.8	1.2	8.4
GB425-14	49.2	73.3	32.5	62.1	5.5	50.2	730	65.4	7.6	n.d	299	5.7	2.2	1.6	11.9
GB425-15	47.8	24.5	5.5	34.5	18.7	35.8	1420	37.4	1.0	0.3	16600	3.6	1.8	11.5	9.6
GB425-16	52.5	26.5	13.1	35.9	21.9	61.4	1580	42.8	2.4	1.0	27700	4.6	2.2	2.1	12.4
GB425-17	49.5	24.3	8.5	36.9	18.6	44.5	1460	39.4	1.6	0.7	23800	4.4	2.1	10.3	10.5
GB425-18	63.0	26.3	9.0	52.6	13.0	32.8	849	40.6	2.9	0.5	3850	4.9	2.0	3.8	15.0
GB425-19	66.4	27.1	6.0	34.1	16.6	61.0	965	42.8	1.7	0.5	12300	4.5	2.3	12.2	16.1
GB425-20	61.7	33.2	8.5	42.5	15.0	38.3	1050	49.7	2.1	0.9	10100	5.1	2.3	8.8	10.0
GB425-21	45.5	21.9	9.5	40.6	10.4	32.1	896	35.2	2.6	0.8	4220	3.6	1.5	4.8	7.5
GB425-22	57.8	23.8	7.1	50.1	15.1	41.6	946	38.3	1.8	1.3	6560	5.1	1.9	13.2	15.3
GB425-23	51.3	69.7	6.6	64.8	14.4	35.8	555	42.3	2.5	1.0	1700	20.7	1.9	1.5	18.8
GB425-24	111.0	24.6	13.6	51.0	12.6	53.3	672	36.6	3.3	1.9	3560	6.0	2.1	1.9	105.2

n.d: no data.

References

Aharon, P., Schwarcz, H.P., Roberts, H.H., 1997. Radiometric dating of submarine hydrocarbon seeps in the Gulf of Mexico. Geol. Soc. Am. Bull. 109, 568–579.

Algeo, T., Tribovillard, N., 2009. Environmental analysis of paleoceanographic systems based on molybdenum–uranium covariation. Chem. Geol. 268, 211–225.

Bau, M., Dulski, P., 1996. Distribution of yttrium and rare-earth elements in the Penge and Kuruman iron-formations, Transvaal Supergroup, South Africa. Precambrian Res. 79, 37–55.

Bayon, G., Henderson, G., Bohn, M., 2009. U–Th stratigraphy of a cold seep carbonate crust. Chem. Geol. 260, 47–56.

Bayon, G., Birot, D., Ruffine, L., Caprais, J.C., Ponzevera, E., Bollinger, C., Donval, J.P., Charlou, J.L., Voisset, M., Grimaud, S., 2011. Evidence for intense REE scavenging at cold seeps from the Niger Delta margin. Earth Planet. Sci. Lett. 312, 443–452.

Bayon, G., Dupré, S., Ponzevera, E., Etoubleau, J., Chéron, S., Pierre, C., Mascle, J., Boetius, A., De Lange, G.J., 2013. Formation of carbonate chimneys in the Mediterranean Sea linked to deep-water oxygen depletion. Nat. Geosci. 6, 755–760.

Berner, R.A., 1980. Early Diagenesis — A Theoretical Approach. , Princeton University Press, Princeton.

Bian, Y., Feng, D., Roberts, H.H., Chen, D., 2013. Tracing the evolution of seep fluids from authigenic carbonates: Green Canyon, northern Gulf of Mexico. Mar. Pet. Geol. 44, 71–81.
Birgel, D., Feng, D., Roberts, H.H., Peckmann, J., 2011. Changing redox conditions at cold seeps as revealed by authigenic carbonates from Alaminos Canyon, northern Gulf of Mexico. Chem. Geol. 285, 82–96.
Boetius, A., Ravenschlag, K., Schubert, C.J., Rickert, D., Widdel, F., Gieseke, A., Amann, R., Jørgensen, B.B., Witte, U., Pfannkuche, O., 2000. A marine microbial consortium apparently mediating anaerobic oxidation of methane. Nature 407, 623–626.
Bohrmann, G., Greinert, J., Suess, E., Torres, M., 1998. Authigenic carbonates from the Cascadia subduction zone and their relation to gas hydrate stability. Geology 26, 647–650.
Böning, P., Brumsack, H.-J., Schnetger, B., Grunwald, M., 2009. Trace element signatures of Chilean upwelling sediments at ~36°S. Mar. Geol. 259, 112–121.
Burton, E.A., 1993. Controls on marine carbonate cement mineralogy: review and reassessment. Chem. Geol. 105, 163–179.
Calvert, S.E., Price, N.B., 1977. Geochemical variation in ferromanganese nodules and associated sediments from the Pacific Ocean. Mar. Chem. 5, 43–74.
Campbell, K.A., 2006. Hydrocarbon seep and hydrothermal vent paleoenvironments and paleontology: past developments and future research directions. Palaeogeogr. Palaeoclimatol. Palaeoecol. 232, 362–407.
Cangemi, M., Di Leonardo, R., Bellanca, A., Cundy, A., Neri, R., Angelone, M., 2010. Geochemistry and mineralogy of sediments and authigenic carbonates from the Malta Plateau, Strait of Sicily (Central Mediterranean): relationships with mud/fluid release from a mud volcano system. Chem. Geol. 276, 294–308.
Castellini, D.G., Dickens, G.R., Snyder, G.T., Ruppel, C.D., 2006. Barium cycling in shallow sediment above active mud volcanoes in the Gulf of Mexico. Chem. Geol. 226, 1–30.
Chaillou, G., Schäfer, J., Blanc, G., Anschutz, P., 2008. Mobility of Mo, U, As, and Sb within modern turbidites. Mar. Geol. 254, 171–179.
Charlou, J.L., Donval, J.P., Fouquet, Y., Ondreas, H., Knoery, J., Cochonat, P., Levaché, D., Poirier, Y., Jean-Baptiste, P., Fourré, E., Chazallon, B., 2004. Physical and chemical characterization of gas hydrates and associated methane plumes in the Congo–Angola Basin. Chem. Geol. 205, 405–425.
Chen, D.F., Huang, Y.Y., Yuan, X.L., Cathles, L.M., 2005. Seep carbonates and preserved methane oxidizing archaea and sulfate reducing bacteria fossils suggest recent gas venting on the seafloor in the Northeastern South China Sea. Mar. Pet. Geol. 22, 613–621.
Cutter, G.A., Cutter, L.S., Featherstone, A.M., Lohrenz, S.E., 2001. Antimony and arsenic biogeochemistry in the western Atlantic Ocean. Deep-Sea Res. II Top. Stud. Oceanogr. 48, 2895–2915.
Dekov, V.M., Scholten, J.C., Botz, R., Garbe-Schönberg, C.D., Stoffers, P., 2007. Fe–Mn-(hydr)oxide-carbonate crusts from the Kebrit Deep, Red Sea: precipitation at the seawater/brine redoxcline. Mar. Geol. 236, 95–119.
Dellwig, O., Leipe, T., März, C., Glockzin, M., Pollehne, F., Schnetger, B., Yakushev, E.V., Böttcher, M.E., Brumsack, H.-J., 2010. A new particulate Mn–Fe–P-shuttle at the redoxcline of anoxic basins. Geochim. Cosmochim. Acta 74, 7100–7115.
Droz, L., Rigaut, F., Cochonat, P., Tofani, R., 1996. Morphology and recent evolution of the Zaire turbidite system (Gulf of Guinea). Geol. Soc. Am. Bull. 108, 253–269.
Feng, D., Chen, D., Qi, L., Roberts, H.H., 2008. Petrographic and geochemical characterization of seep carbonate from Alaminos Canyon, Gulf of Mexico. Chin. Sci. Bull. 53, 1716–1724.
Feng, D., Chen, D., Peckmann, J., 2009a. Rare earth elements in seep carbonates as tracers of variable redox conditions at ancient hydrocarbon seeps. Terra Nova 21, 49–56.
Feng, D., Chen, D., Roberts, H.H., 2009b. Petrographic and geochemical characterization of seep carbonate from Bush Hill (GC 185) gas vent and hydrate site of the Gulf of Mexico. Mar. Pet. Geol. 26, 1190–1198.
Feng, D., Chen, D., Peckmann, J., Bohrmann, G., 2010a. Authigenic carbonates from methane seeps of the northern Congo fan: microbial formation mechanism. Mar. Pet. Geol. 27, 748–756.
Feng, D., Roberts, H.H., Cheng, H., Peckmann, J., Bohrmann, G., Lawrence Edwards, R., Chen, D., 2010b. U/Th dating of cold-seep carbonates: an initial comparison. Deep-Sea Res. II Top. Stud. Oceanogr. 57, 2055–2060.
Feng, D., Lin, Z., Bian, Y., Chen, D., Peckmann, J., Bohrmann, G., Roberts, H.H., 2013. Rare earth elements of seep carbonates: indication for redox variations and microbiological processes at modern seep sites. J. Asian Earth Sci. 65, 27–33.
Gay, A., Lopez, M., Cochonat, P., Levaché, D., Sermondadaz, G., Seranne, M., 2006. Evidences of early to late fluid migration from an upper Miocene turbiditic channel revealed by 3D seismic coupled to geochemical sampling within seafloor pockmarks, Lower Congo Basin. Mar. Pet. Geol. 23, 387–399.
Gay, A., Lopez, M., Berndt, C., Seranne, M., 2007. Geological controls on focused fluid flow associated with seafloor seeps in the Lower Congo Basin. Mar. Geol. 244, 68–92.
Ge, L., Jiang, S.-Y., Swennen, R., Yang, T., Yang, J.-H., Wu, N.-Y., Liu, J., Chen, D.-H., 2010. Chemical environment of cold seep carbonate formation on the northern continental slope of South China Sea: evidence from trace and rare earth element geochemistry. Mar. Geol. 277, 21–30.
González, F.J., Somoza, L., León, R., Medialdea, T., de Torres, T., Ortiz, J.E., Lunar, R., Martínez-Frías, J., Merinero, R., 2012. Ferromanganese nodules and microhardgrounds associated with the Cadiz Contourite Channel (NE Atlantic): palaeoenvironmental records of fluid venting and bottom currents. Chem. Geol. 310–311, 56–78.
Greinert, J., Bohrmann, G., Suess, E., 2001. Gas hydrate-associated carbonates and methane-venting at Hydrate Ridge: classification, distribution, and origin of authigenic lithologies. Geophysical Monographs, 124. American Geophysical Union, Washington DC pp. 131–143.
Haas, A., Peckmann, J., Elvert, M., Sahling, H., Bohrmann, G., 2010. Patterns of carbonate authigenesis at the Kouilou pockmarks on the Congo deep-sea fan. Mar. Geol. 268, 129–136.
Haley, B.A., Klinkhammer, G.P., McManus, J., 2004. Rare earth elements in pore waters of marine sediments. Geochim. Cosmochim. Acta 68, 1265–1279.
Helz, G., Miller, C., Charnock, J., Mosselmans, J., Pattrick, R., Garner, C., Vaughan, D., 1996. Mechanism of molybdenum removal from the sea and its concentration in black shales: EXAFS evidence. Geochim. Cosmochim. Acta 60, 3631–3642.
Helz, G.R., Bura-Nakić, E., Mikac, N., Ciglenečki, I., 2011. New model for molybdenum behavior in euxinic waters. Chem. Geol. 284, 323–332.
Himmler, T., Bach, W., Bohrmann, G., Peckmann, J., 2010. Rare earth elements in authigenic methane-seep carbonates as tracers for fluid composition during early diagenesis. Chem. Geol. 277, 126–136.
Himmler, T., Haley, B.A., Torres, M.E., Klinkhammer, G.P., Bohrmann, G., Peckmann, J., 2013. Rare earth element geochemistry in cold-seep pore waters of Hydrate Ridge, northeast Pacific Ocean. Geo-Mar. Lett. 33, 369–379.
Hinrichs, K.-U., Hayes, J.M., Sylva, S.P., Brewer, P.G., DeLong, E.F., 1999. Methane-consuming archaebacteria in marine sediments. Nature 398, 802–805.
Joye, S.B., Samarkin, V.A., 2009. Metabolic variability in seafloor brines revealed by carbon and sulphur dynamics. Nat. Geosci. 2, 349–354.
Joye, S., MacDonald, I., Montoya, J.P., Peccini, M., 2005. Geophysical and geochemical signatures of Gulf of Mexico seafloor brines. Biogeosciences 2, 295–309.
Judd, A., Hovland, M., 2007. Seabed Fluid Flow, Cambridge University Press, Cambridge.
Kim, J.-H., Torres, M.E., Haley, B.A., Kastner, M., Pohlman, J.W., Riedel, M., Lee, Y.-J., 2012. The effect of diagenesis and fluid migration on rare earth element distribution in pore fluids of the northern Cascadia accretionary margin. Chem. Geol. 291, 152–165.
Klaucke, I., Weinrebe, W., Petersen, C.J., Bowden, D., 2010. Temporal variability of gas seeps offshore New Zealand: multi-frequency geoacoustic imaging of the Wairarapa area, Hikurangi margin. Mar. Geol. 272, 49–58.
Koschinsky, A., Hein, J.R., 2003. Uptake of elements from seawater by ferromanganese crusts: solid-phase associations and seawater speciation. Mar. Geol. 198, 331–351.
Kowalski, N., Dellwig, O., Beck, M., Gräwe, U., Neubert, N., Nägler, T.F., Badewien, T.H., Brumsack, H.-J., van Beusekom, J.E.E., Böttcher, M.E., 2013. Pelagic molybdenum concentration anomalies and the impact of sediment resuspension on the molybdenum budget in two tidal systems of the North Sea. Geochim. Cosmochim. Acta 119, 198–211.
Luff, R., Wallmann, K., 2003. Fluid flow, methane fluxes, carbonate precipitation and biogeochemical turnover in gas hydrate-bearing sediments at Hydrate Ridge, Cascadia Margin: numerical modeling and mass balances. Geochim. Cosmochim. Acta 67, 3403–3421.
MacDonald, I.R., Buthman, D.B., Sager, W.W., Peccini, M.B., Guinasso, N.L., 2000. Pulsed oil discharge from a mud volcano. Geology 28, 907–910.
Marton, L.G., Tari, G.C., Lehmann, C.T., 2000. Evolution of the Angolan passive margin, West Africa, with emphasis on post-salt structural style. In: Mohriak, W., Talwani, M. (Eds.), Atlantic Rifts and Continental Margins. Geophysical Monograph, 115. AGU, pp. 129–149.
McLennan, S., 1989. Rare earth elements in sedimentary rocks: influence of provenance and sedimentary processes. Rev. Mineral. Geochem. 21, 169–200.
McLennan, S.M., 2001. Relationships between the trace element composition of sedimentary rocks and upper continental crust. Geochem. Geophys. Geosyst. 2 (2000GC000109). http://dx.doi.org/10.1029/2000GC000109.
Milkov, A.V., Sassen, R., 2000. Thickness of the gas hydrate stability zone, Gulf of Mexico continental slope. Mar. Pet. Geol. 17, 981–991.
Morford, J.L., Emerson, S., 1999. The geochemistry of redox sensitive trace metals in sediments. Geochim. Cosmochim. Acta 63, 1735–1750.
Nägler, T.F., Neubert, N., Böttcher, M.E., Dellwig, O., Schnetger, B., 2011. Molybdenum isotope fractionation in pelagic euxinia: evidence from the modern Black and Baltic Seas. Chem. Geol. 289, 1–11.
Nath, B., Jean, J.S., Lee, M.K., Yang, H.J., Liu, C.C., 2008. Geochemistry of high arsenic groundwater in Chia-Nan plain, Southwestern Taiwan: possible sources and reactive transport of arsenic. J. Contam. Hydrol. 99, 85–96.
Neubert, N., Nagler, T.F., Böettcher, M.E., 2008. Sulfidity controls molybdenum isotope fractionation into euxinic sediments: evidence from the modern Black Sea. Geology 36, 775–778.
Nöthen, K., Kasten, S., 2011. Reconstructing changes in seep activity by means of pore water and solid phase Sr/Ca and Mg/Ca ratios in pockmark sediments of the Northern Congo Fan. Mar. Geol. 287, 1–13.
Palomares, R.M., Hernandez, R.L., Frias, J.M., 2012. Mechanisms of trace metal enrichment in submarine, methane-derived carbonate chimneys from the Gulf of Cadiz. J. Geochem. Explor. 112, 297–305.
Peckmann, J., Thiel, V., 2004. Carbon cycling at ancient methane-seeps. Chem. Geol. 205, 443–467.
Peckmann, J., Reimer, A., Luth, U., Luth, C., Hansen, B., Heinicke, C., Hoefs, J., Reitner, J., 2001. Methane-derived carbonates and authigenic pyrite from the northwestern Black Sea. Mar. Geol. 177, 129–150.
Peckmann, J., Birgel, D., Kiel, S., 2009. Molecular fossils reveal fluid composition and flow intensity at a Cretaceous seep. Geology 37, 847–850.
Peketi, A., Mazumdar, A., Joshi, R., Patil, D., Srinivas, P., Dayal, A., 2012. Tracing the Paleo sulfate-methane transition zones and H_2S seepage events in marine sediments: an application of C–S–Mo systematics. Geochem. Geophys. Geosyst. 13, Q10007. http://dx.doi.org/10.1029/2012GC004288.
Pourret, O., Davranche, M., Gruau, G., Dia, A., 2008. New insights into cerium anomalies in organic-rich alkaline waters. Chem. Geol. 251, 120–127.
Qi, L., Zhou, M.F., Malpas, J., Sun, M., 2005. Determination of rare earth elements and Y in ultramafic rocks by ICP-MS after preconcentration using $Fe(OH)_3$ and $Mg(OH)_2$ coprecipitation. Geostand. Geoanal. Res. 29, 131–141.

Roberts, H.H., Aharon, P., 1994. Hydrocarbon-derived carbonate buildups of the northern Gulf of Mexico continental slope: a review of submersible investigations. Geo-Mar. Lett. 14, 135–148.
Roberts, H.H., Carney, R.S., 1997. Evidence of episodic fluid, gas, and sediment venting on the northern Gulf of Mexico continental slope. Econ. Geol. Bull. Soc. Econ. Geol. 92, 863–879.
Roberts, H.H., Feng, D., Joye, S.B., 2010a. Cold-seep carbonates of the middle and lower continental slope, northern Gulf of Mexico. Deep-Sea Res. II Top. Stud. Oceanogr. 57, 2040–2054.
Roberts, H., Shedd, W., Hunt Jr., J., 2010b. Dive site geology: DSV ALVIN (2006) and ROV JASON II (2007) dives to the middle-lower continental slope, northern Gulf of Mexico. Deep-Sea Res. II Top. Stud. Oceanogr. 57, 1837–1858.
Rongemaille, E., Bayon, G., Pierre, C., Bollinger, C., Chu, N.C., Fouquet, Y., Riboulot, V., Voisset, M., 2011. Rare earth elements in cold seep carbonates from the Niger delta. Chem. Geol. 286, 196–206.
Sahling, H., Bohrmann, G., Spiess, V., Bialas, J., Breitzke, M., Ivanov, M., Kasten, S., Krastel, S., Schneider, R., 2008. Pockmarks in the Northern Congo Fan area, SW Africa: complex seafloor features shaped by fluid flow. Mar. Geol. 249, 206–225.
Sassen, R., MacDonald, I.R., 1994. Evidence of structure H hydrate, Gulf of Mexico continental slope. Org. Geochem. 22, 1029–1032.
Sassen, R., Sweet, S.T., Milkov, A.V., DeFreitas, D.A., Salata, G.G., McDade, E.C., 1999. Geology and geochemistry of gas hydrates, central Gulf of Mexico continental slope. Gulf Coast Assoc. Geol. Soc. Trans. 49, 462–468.
Sato, H., Hayashi, K.-i., Ogawa, Y., Kawamura, K., 2012. Geochemistry of deep sea sediments at cold seep sites in the Nankai Trough: insights into the effect of anaerobic oxidation of methane. Mar. Geol. 323–325, 47–55.
Scott, C., Lyons, T.W., 2012. Contrasting molybdenum cycling and isotopic properties in euxinic versus non-euxinic sediments and sedimentary rocks: refining the paleoproxies. Chem. Geol. 324–325, 19–27.
Shields, G., Kimura, H., Yang, J., Gammon, P., 2004. Sulphur isotopic evolution of Neoproterozoic–Cambrian seawater: new francolite-bound sulphate $\delta^{34}S$ data and a critical appraisal of the existing record. Chem. Geol. 204, 163–182.
Solomon, E.A., Kastner, M., Jannasch, H., Robertson, G., Weinstein, Y., 2008. Dynamic fluid flow and chemical fluxes associated with a seafloor gas hydrate deposit on the northern Gulf of Mexico slope. Earth Planet. Sci. Lett. 270, 95–105.
Taylor, S.R., McLennan, S.M., 1985. The Continental Crust: Its Composition and Evolution. Blackwell, Oxford (312 pp.).
Teichert, B., Eisenhauer, A., Bohrmann, G., Haase-Schramm, A., Bock, B., Linke, P., 2003. U/Th systematics and ages of authigenic carbonates from Hydrate Ridge, Cascadia Margin: recorders of fluid flow variations. Geochim. Cosmochim. Acta 67, 3845–3857.
Tong, H., Feng, D., Cheng, H., Yang, S., Wang, H., Min, A.G., Edwards, R.L., Chen, Z., Chen, D., 2013. Authigenic carbonates from seeps on the northern continental slope of the South China Sea: new insights into fluid sources and geochronology. Mar. Pet. Geol. 43, 260–271.
Tribovillard, N., Algeo, T.J., Lyons, T., Riboulleau, A., 2006. Trace metals as paleoredox and paleoproductivity proxies: an update. Chem. Geol. 232, 12–32.
Tribovillard, N., Algeo, T.J., Baudin, F., Riboulleau, A., 2012a. Analysis of marine environmental conditions based on molybdenum–uranium covariation—applications to Mesozoic paleoceanography. Chem. Geol. 324–325, 46–58.
Tribovillard, N., Sansjofre, P., Ader, M., Trentesaux, A., Averbuch, O., Barbecot, F., 2012b. Early diagenetic carbonate bed formation at the sediment–water interface triggered by synsedimentary faults. Chem. Geol. 300–301, 1–13.
Tribovillard, N., du Châtelet, E.A., Gay, A., Barbecot, F., Sansjofre, P., Potdevin, J.-L., 2013. Geochemistry of cold seepage-impacted sediments: per-ascensum or per-descensum trace metal enrichment? Chem. Geol. 340, 1–12.
Trudgill, B.D., Rowan, M.G., Fiduk, J.C., Weimer, P., Gale, P.E., Korn, B.E., Phair, R.L., Gafford, W.T., Roberts, G.R., Dobbs, S.W., 1999. The Perdido fold belt, northwestern deep Gulf of Mexico; part 1, structural geometry, evolution and regional implications. AAPG Bull. 83, 88–113.
Tryon, M.D., Brown, K.M., 2004. Fluid and chemical cycling at Bush Hill: implications for gas-and hydrate-rich environments. Geochem. Geophys. Geosyst. 5, 1–7.
Tryon, M.D., Brown, K.M., Torres, M.E., Tréhu, A.M., McManus, J., Collier, R.W., 1999. Measurements of transience and downward fluid flow near episodic methane gas vents, Hydrate Ridge, Cascadia. Geology 27, 1075–1078.
Van der Weijden, C.H., 2002. Pitfalls of normalization of marine geochemical data using a common divisor. Mar. Geol. 184, 167–187.
Voegelin, A.R., Nägler, T.F., Samankassou, E., Villa, I.M., 2009. Molybdenum isotopic composition of modern and Carboniferous carbonates. Chem. Geol. 265, 488–498.
Wang, S., Xu, L., Zhao, Z., Wang, S., Jia, Y., Wang, H., Wang, X., 2012. Arsenic retention and remobilization in muddy sediments with high iron and sulfur contents from a heavily contaminated estuary in China. Chem. Geol. 314, 57–65.
Zheng, Y., Anderson, R.F., van Geen, A., Kuwabara, J., 2000. Authigenic molybdenum formation in marine sediments: a link to pore water sulfide in the Santa Barbara Basin. Geochim. Cosmochim. Acta 64, 4165–4178.
Zheng, Y., Anderson, R.F., van Geen, A., Fleisher, M.Q., 2002. Remobilization of authigenic uranium in marine sediments by bioturbation. Geochim. Cosmochim. Acta 66, 1759–1772.